Preprints of the 21st IFAC World Congress (Virtual)
Berlin, Germany, July 12-17, 2020

Modelling, Implementation and Control of a Wind Musical Instrument

Gaby ABOU HAIDAR[1,2]
[1]Bordeaux University, CNRS, IMS Lab.
33600 Talence, Bordeaux, France
[2]American University of Science and Technology, Faculty of Engineering
Zahle, Lebanon
gabouhaidar@aust.edu.lb

Xavier MOREAU
Bordeaux University, CNRS, IMS Lab.
33600 Talence, Bordeaux, France
xavier.moreau@u-bordeaux.fr

Roy ABI ZEID DAOU[3,4]
[3]Lebanese German University,
Biomedical technologies department,
Jounieh, Lebanon
r.abizeiddaou@lgu.edu.lb
[4]MART, Learning, Education and Training Center, Chananiir, Lebanon
roydaou@mart-ler.org

***Abstract* – This paper presents the second part of a larger project whose final objective is the study of viscous thermal losses in a wind musical instrument from a hardware-in-the-loop simulation platform. After the realization of the platform in the first part of this project, the objective of the second part, presented in this paper, is to adjust the dynamic behaviour of the numerical simulator with respect to the real dynamic behaviour of the test bench. So, in this paper, the different parts that constitute the platform are recalled, and the modelling/validation of each part are described. A control-oriented model is derived. The control architecture is designed for a robust control of the artificial mouth. The robust controller method uses CRONE system design methodology. The investigations show that the design of the artificial mouth and of its controller provides very good dynamic performances.**

***Keywords* – Wind musical instrument; Viscous thermal losses; Artificial Mouth; CRONE system design methodology**

I. INTRODUCTION

Blowing machines, so-called artificial mouths, are used in musical acoustics when studying wind instruments, at least since 80 years [1]. As proposed in the literature review [2] [3] [4] [5] [6] [7] [8], the objective of controlling the pressure inside the artificial mouth is considered in many applications:

- to ensure quasi-static variation in order to analyse experimental bifurcation diagrams;
- to reproduce typical signals (Heaviside step function, sinus, ramps,…) to compare the dynamics of the real instrument to the one obtained through numerical simulations;
- to mimic the temporal evolutions recorded on real musicians in order to analyse the strategies discovered over the years of practice.

The objective of our project is the study of viscous thermal losses in a wind musical instrument from a hardware-in-the-loop simulation platform. The hardware part of the platform is made up of an automatic blowing machine connected to the mouthpiece of a wind instrument [9] [10]. The software part of the platform is composed of resonator numerical model of the wind instrument including viscous thermal losses based on fractional model and the Control System (CS) used for regulating the pressure inside the artificial mouth. The first part of the project was the Computer Aided Design (CAD) of the platform. Thus, a digital simulator was developed with MatLab/Simulink software based on wind instruments artificial mouths found in several publications [1] [2]. The second part, presented in this paper, is based on the realization of the test bench from the first part. The objective is to adjust the dynamic behaviour of the numerical simulator to the real dynamic behaviour of test bench. The third and last part consists in modelling and analysing the viscous thermal losses present in the resonator of the wind instrument from fractional models [11].

So, this paper is organized as follows. In section II, the different components that constitute the platform are presented. In section III, the specifications for the control of the pressure inside the artificial mouth are given and explained. In section IV, the modelling and the validation of each component are described. In section V, CRONE system design methodology is displayed in order to control the pressure. Section VI presents the results that provide very good dynamic performances. At the end, section VII concludes this paper and proposes some future works concerning the third and last part of the project.

II. SYSTEM DESCRIPTION

The test bench considered in this paper is presented in figure 1. A servo-valve is connected to an air compressor through a pressure reducer. The maximum pressure available is around 6 bars, and the pressure reducer (with its manometer) is used to adjust the pressure P_1 upstream the servo-valve. The servo-valve is connected at the entrance of the artificial mouth itself whose internal volume $V = 343$ cm^3 is the place where the air pressure P_m must be controlled. The artificial mouth blows into the mouthpiece of a recorder flute. A MatLab/Simulink/LabVIEW program is used in order to control the air pressure P_m. Added to that, a flow meter, a temperature and a pressure transducers are used in order to characterize the behaviour of the different parts of this system.

Figure 2 presents the scheme of the experimental setup and figure 3 the block diagram associated.

Remark

For the rest of the paper, the following notation is adopted for a variable X(t):

$$X(t) = X^e + x(t) \quad ,(1)$$

where X^e is a constant value fixed by a given operating point and x(t) the fluctuation around X^e. Moreover, $\tilde{X}(t)$

Copyright lies with the authors

represents a measurement of X(t) and $\hat{X}(t)$ *an estimate of X(t).*

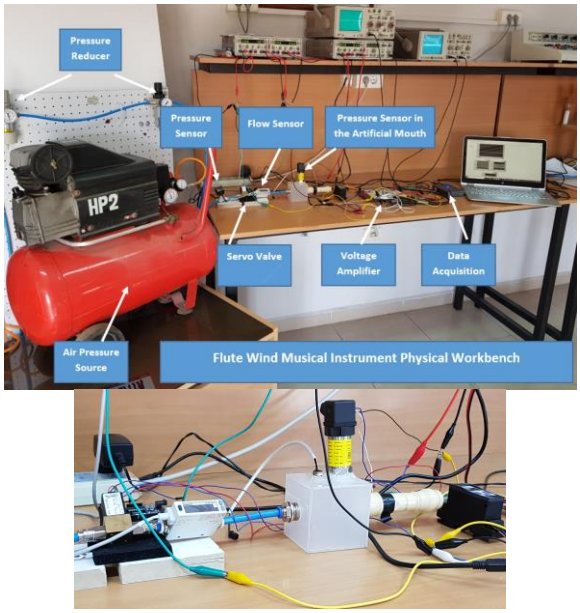

Fig. 1. Photos of the test bench

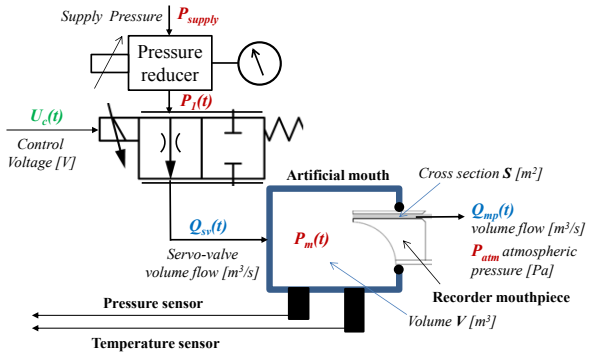

Fig. 2. Scheme of the experimental setup

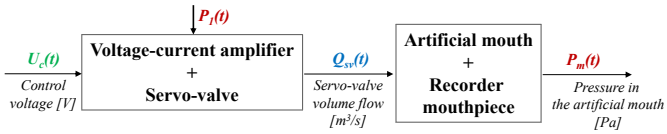

Fig. 3. Block diagram of the experimental setup

III. Specifications For The Control

In the classical use of an artificial mouth, the pressure $P_m(t) = P_m^e + p_m(t)$ upstream the mouthpiece of the recorder flute (inside the artificial mouth) is tuned by hand through the pressure reducer and its manometer. When the compressed air is produced by a compressor such as that presented in figure 1, the pressure $P_1(t) = P_1^e + p_1(t)$ upstream the servo-valve, fluctuates because the compressor tank being in need to be recharged once its pressure becomes below a certain level. This is the reason why it is difficult to manually control the pressure. Thus, the purpose of automatic pressure control inside the artificial mouth is to increase the accuracy by rejecting the pressure fluctuation $p_1(t)$ considered as a disturbance, while satisfying robust tracking of the reference pressure $P_{ref}(t)$ [1]. To recall, the finality of our project is the study of viscous thermal losses in a wind instrument based on fractional model. In order to facilitate the analysis of this complex problem, the reference pressure is chosen such as:

$$P_{ref}(t) = P_{ref}^e + p_{ref}(t) = P_{ref}^e + P_{ref}^0 \cos(2\pi f_0 t). \quad (2)$$

For all these reasons, the architecture of the control system presented in figure 4 consists of a $P_{ref}(t)$ reference generator, a $U_{ff}(t)$ feedforward control and a $U_{fb}(t)$ feedback control, the robust controller of which is designed with the CRONE methodology [12] [13] [14] [15] [16].

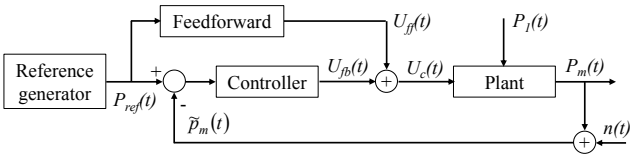

Fig. 4. Architecture of the Control System (CS)

IV. System Modelling And Validation

As presented in figure 3, the experimental setup is divided into two parts:

- The first one consists of a voltage-current amplifier, a servo-valve connected to an air compressor via a pressure reducer. The inputs of this part are $P_1(t)$ the pressure upstream the servo-valve and $U_c(t) = U_{ff}(t) + U_{fb}(t)$ the control signal generated from MatLab/Simulink/LabVIEW, whereas the output is $Q_{sv}(t)$ the flow rate delivered by the servo-valve. This last device presents a nonlinear behaviour;
- The second part is the artificial mouth and the mouthpiece of the recorder flute. The input of this part is $Q_{sv}(t)$ the flow rate from the servo-valve, whereas the output is $\tilde{P}_m(t)$ the pressure measured within the artificial mouth, $\tilde{P}_m(t) = P_m(t) + n(t)$ where $n(t)$ is s measurement noise.

A. Modelling and validation of the servo-valve

The servo-valve is designed by Bürkert firm (ref. Bürkert 2871). Based on previous works [1] [2] [9] [10], it has been shown that the servo-valve's behaviour can be divided in two parts: a nonlinear static part and a linear dynamic part.

Figure 5 shows the block diagram of the servo-valve. In order to express the output of the nonlinear part, a static flow Q_{stat} is introduced.

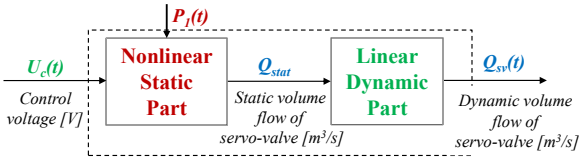

Fig. 5. Block diagram of the servo-valve

The linear dynamic part between Q_{stat} and $Q_{sv}(t)$ is represented by a second order transfer function $H_{sv}(s)$ with a unit static gain [1] [2] [9] [10]:

$$H_{sv}(s) = \frac{1}{1 + 2\zeta\, s/\omega_0 + (s/\omega_0)^2}, \quad (3)$$

where $\zeta = 0.3$ and $\omega_0 = 2\pi\, 240$ rad/s.

As already mentioned, the output flow rate $Q_{sv} = f(U_c, P_1)$ depends on the control voltage signal U_c (that may vary

between 0 and 10V) and the pressure P_1 upstream the servo-(max[P_1] = 6 bar).

Figure 6 shows the static operating domain obtained from measurements for $U_c \in [0\,;10]$ V and $P_1 \in [1\,;6]$ bar .

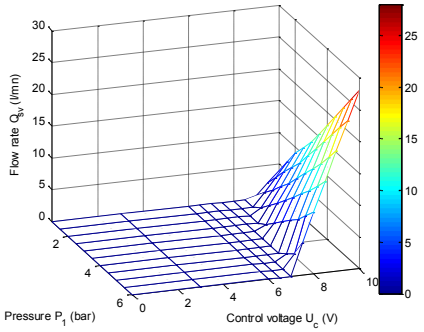

Fig. 6. Static operating domain obtained from measurements

We can see a dead zone where $Q_{sv} = 0$ whatever the value of $U_c \in [0\,;U_{\min}(P_1)]$, and a variation zone of Q_{sv} where the saturation, max[Q_{sv}], depends on max[U_c] = 10 V and max[P_1] = 6 bar. In the variation zone, for a given operating point O defined by $O \equiv \left(U_c^e\,;P_1^e\right)$, the flow rate $Q_{sv}(t, U_c, P_1)$ can be written as follow:

$$Q_{sv}(t,U_c,P_1) = Q_{sv}^e\left(U_c^e,P_1^e\right) + q_{sv}(t,U_c,P_1), \quad (4)$$

where

$$q_{sv}(t,U_c,P_1) = K_{qu}\left(U_c^e,P_1^e\right)\,u_c(t) + K_{qp}\left(U_c^e,P_1^e\right)\,p_1(t) \quad (5)$$

and $$K_{qu}\left(U_c^e,P_1^e\right) = \left.\frac{\partial Q_{sv}}{\partial u_c}\right|_{\substack{U_c^e\\P_1^e}},\quad K_{qp}\left(U_c^e,P_1^e\right) = \left.\frac{\partial Q_{sv}}{\partial p_1}\right|_{\substack{U_c^e\\P_1^e}} \quad (6)$$

The estimated value $\hat{K}_{qu}$ of the static gain K_{qu} is obtained from:

$$\underset{[\text{l.mn}^{-1}.\text{V}^{-1}]}{\hat{K}_{qu}(P_1)} = \frac{\Delta\tilde{Q}_{sv}}{\Delta U_c(P_1)} = \frac{\max\left[\tilde{Q}_{sv}(U_{\max},P_1)\right]-0}{\max[U_c]-U_{\min}(P_1)}, \quad (7)$$

with $U_{max} = \max[U_c] = 10$ V.

Figure 7 shows the variation of $\hat{K}_{qu}$ versus $P_1 \in [1\,;6]$ bar that can be considered as linear and modelled by

$$\underset{[\text{l.mn}^{-1}.\text{V}^{-1}]}{\hat{K}_{qu}(P_1)} = \underset{[\text{bar}]}{A}\;P_1 + B, \quad (8)$$

with $$\begin{cases} A = 0.99 \;\; \text{l.mn}^{-1}.\text{V}^{-1}.\text{bar}^{-1} \\ B = 3.4 \;\; \text{l.mn}^{-1}.\text{V}^{-1} \end{cases}. \quad (9)$$

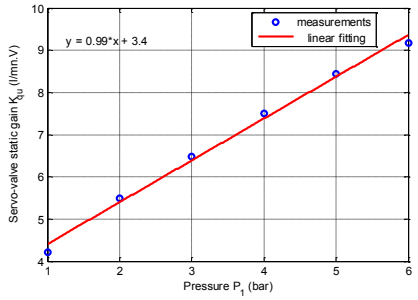

Fig. 7. Variation of $\hat{K}_{qu}$ versus $P_1 \in [1\,;6]$ bar

B. Choice of an operating point

The limits of the servo-valve operating domain being estimated, the choice of an operating point $O \equiv \left(U_c^e\,;P_1^e\right)$ and the amplitude of the variations around this point is essential in order to avoid the risks of saturation of the flow rate $Q_{sv}(t)$.

After observing the pressure $P_1(t)$ during numerous tests, the fluctuations $p_1(t)$ are considered to be limited between -1 and + 1bar. This is the reason why we chose $P_1^e = 5$ bar , and so $P_1 \in [4\,;6]$ bar . For this variation range of P_1, the variation range of U_c without saturation of Q_{sv} has as limits $U_{\min}(P_{1\min} = 4\text{bar}) = 7.55$ V and $U_{max} = 10$ V, so:

$$7.55\text{ V} \le U_c(t) = U_{ff}(t) + U_{fb}(t) \le 10\text{ V}, \quad (10)$$

with $$U_{ff}(t) = U_c^e + U_c^0\cos(2\pi\,f_0). \quad (11)$$

By choosing $U_c^e = 8.5$ V and $U_c^0 = 0.5$ V , the variation range of the feed-forward control signal U_{ff} is given by:

$$\begin{cases} \max\left[U_{ff}(t)\right] = U_c^e + U_c^0 = 9\text{ V} \le U_{\max} = 10\text{ V} \\ \min\left[U_{ff}(t)\right] = U_c^e - U_c^0 = 8\text{ V} \ge U_{\min} = 7.55\text{ V} \end{cases}, \quad (12)$$

and the variation range of the feedback control signal U_{fb} is given by:

$$\begin{cases} \max\left[U_{fb}(t)\right] = U_{\max} - \max\left[U_{ff}(t)\right] = +1\text{ V} \\ \min\left[U_{fb}(t)\right] = U_{\min} - \min\left[U_{ff}(t)\right] = -0.45\text{ V} \end{cases}. \quad (13)$$

Figure 8 shows the chosen operating point $O \equiv \left(U_c^e = 8.5\text{ V}\,;P_1^e = 5\text{ bar}\right)$ and the linear static operating domain defined by $U_c \in [7.55\,;10]$ V and $P_1 \in [4\,;6]$ bar .

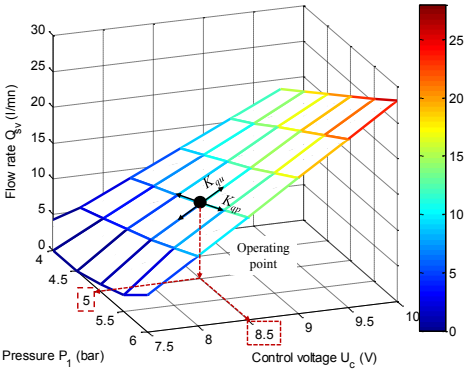

Fig. 8. Operating point O and linear static operating domain

C. Modelling and validation of the Artificial Mouth

The artificial mouth is implemented using a cubic box whose input is the flow rate $Q_{sv}(t)$ coming from the servo-valve and the output is the pressure $P_m(t)$ inside the box. The expression of the pressure $P_m(t)$ is given by the state equation of perfect gases:

$$P_m(t) = \frac{r\,T}{V}\,M(t), \quad (14)$$

where

- $r = 287$ J.kg^{-1}.K^{-1}, the thermodynamic constant of air;
- T =293.5°K, the temperature of air inside the box;

- $M(t)$ is the mass of the air inside the box of volume V. This value depends on the variation of the flow between the input (represented by $Q_{sv}(t)$) and the output (represented by $Q_{mp}(t)$). As small variations are considered, the air density ρ is considered to be constant. Thus, the expression of $M(t)$ is given by:

$$M(t) = \rho \int_0^t \left(Q_{sv}(\tau) - Q_{mp}(\tau)\right) d\tau + M(0), \quad (15)$$

where the expression of $Q_{mp}(t)$ is given by Bernoulli law [2]:

$$Q_{mp}(t) = \alpha \sqrt{\Delta P_{mp}(t)}, \quad (16)$$

where α is a coefficient estimated from measurements and $\Delta P_{mp}(t) = P_m(t) - P_{atm}$ (P_{atm} is the relative atmospheric pressure which is zero by definition, so $\Delta P_{mp}(t) = P_m(t)$). By introducing in relation (15) the pressure $P_m(t)$ from relation (14), namely:

$$P_m(t) = \frac{\rho r T}{V} \int_0^t \left(Q_{sv}(\tau) - Q_{mp}(\tau)\right) d\tau + \frac{r T}{V} M(0), \quad (17)$$

we obtain

$$P_m(t) = \frac{1}{C_{am}} \int_0^t \left(Q_{sv}(\tau) - Q_{mp}(\tau)\right) d\tau + P_m(0), \quad (18)$$

where C_{am} is the pneumatic capacity associated with the volume V of the artificial mouth given by:

$$C_{am} = \frac{V}{\rho r T}, \quad (19)$$

and $P_m(0)$ the initial value of the pressure $P_m(t)$ given by

$$P_m(0) = \frac{r T}{V} M(0). \quad (20)$$

It is important to note that in static $Q^e_{mp} = Q^e_{sv}$, and for a quasi-static variation $Q_{mp}(t) \approx Q_{sv}(t)$.

Figure 9 shows the plot of $Q_{sv}(t)$ versus $P_m(t)^{0.5}$ for a quasi-static variation. The linear fitting (in red) of the measurements (x) leads to an estimate $\hat{\alpha}$ given by:

$$\hat{\alpha} = 1.1 \text{ l.mn}^{-1}.\text{Pa}^{-0.5} = 18.33\,10^{-6} \text{ m}^3.\text{s}^{-1}.\text{Pa}^{-0.5}. \quad (21)$$

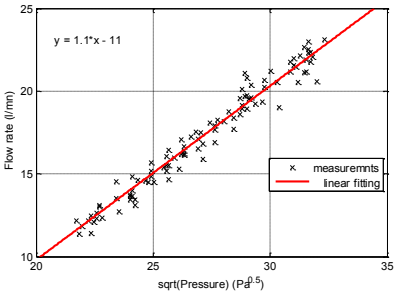

Fig. 9. Plot of $Q_{sv}(t)$ vs sqrt($P_m(t)$) for a quasi-static variation

From relations (16), (17) and (20), the behaviour of the artificial mouth is integrated in the digital simulator programmed with MatLab / Simulink.

C. Linearized model of the plant

In order to design the CRONE controller in frequency domain, a linearized model of the plant is derived around the operating point O. Thus, the pressure $P_m(t)$ and the flow rate $Q_{mp}(t)$ can be expressed as follow:

$$\begin{cases} P_m(t) = P^e_m + p_m(t) \\ Q_{mp}(t) = Q^e_{mp} + q_{mp}(t) \end{cases}, \quad (22)$$

where $Q^e_{mp} = \alpha \sqrt{P^e_m}$ and $q_{mp}(t) = \frac{1}{R_{mp}} p_m(t)$, (23)

with $$\frac{1}{R_{mp}} = \left.\frac{\partial Q_{mp}}{\partial P_m}\right|_{P_m = P^e_m} = \frac{\alpha}{2\sqrt{P^e_m}}. \quad (24)$$

Figure 10 shows the block diagram of the artificial mouth linearized model.

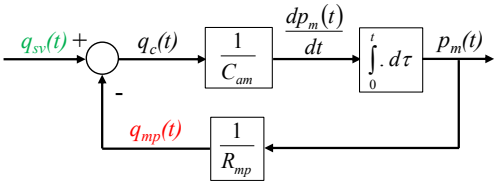

Fig. 10. Block diagram of the artificial mouth linearized model

The transfer function $H_1(s)$ between $\overline{P}_m(s) = \text{LT}\{p_m(t)\}$ and $\overline{Q}_{sv}(s) = \text{LT}\{q_{sv}(t)\}$, where LT represents Laplace Transform, is given by:

$$H_1(s) = \frac{\overline{P}_m(s)}{\overline{Q}_{sv}(s)} = \frac{R_{mp}}{1 + R_{mp} C_{am} s} = \frac{H_0}{1 + s/\omega_1}, \quad (25)$$

where $H_0 = R_{mp}$, $\tau_1 = R_{mp} C_{am}$ and $\omega_1 = 1/\tau_1$. (26)

Finally, the complete linearized model used for the design of the control law is represented by the transfer function $G(s,P_1)$ between $\overline{P}_m(s)$ and $\overline{U}_c(s)$ as follow:

$$G(s,P_1) = \frac{G_0(P_1)}{\left(1 + 2\zeta\, s/\omega_0 + (s/\omega_0)^2\right)(1 + s/\omega_1)}, \quad (27)$$

where $G_0(P_1) = K_{qu}(P_1)\ H_0$. (28)

For the design of the robust control law, the main parameter's values used are:

$$\begin{cases} P_1 \in [4\,;6] \text{ bar}\,;\, P^e_m = 750 \text{ Pa} \\ K_{qu} \in [12.27\,;15.57]\,10^{-5} \text{ m}^3\text{s}^{-1}\text{V}^{-1} \\ \hat{R}_{bec} = 2.65\,10^6 \text{ Pa s m}^{-3}\,;\, C_{am} = 3.38\,10^{-9} \text{ Pa m}^{-3} \\ G_0 \in [325\,;412.5] \text{ Pa V}^{-1}\,;\, \omega_1 = 2\pi\, 17.8 \text{ rad/s} \end{cases}, \quad (29)$$

and three transfer functions are defined for the minimum (4 bar), the nominal (5 bar) and the maximum (6 bar) cases:

$$G_{min}(s, 4 \text{ bar}),\ G_{nom}(s, 5 \text{ bar}),\ G_{max}(s, 6 \text{ bar}). \quad (30)$$

Figure 11 presents the Bode plots of $G(j\omega)$ for three values of the pressure: P_1 = 4 bar (in blue), P_1 = 5 bar (in black) and P_1 = 6 bar (in red).

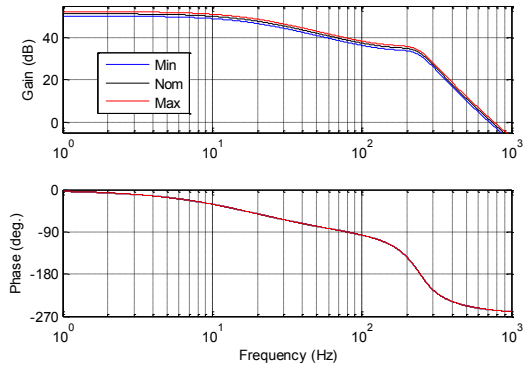

Fig. 11. Bode plots of $G(j\omega)$ for three values of the pressure: P_1 = 4 bar in blue, P_1 = 5 bar in black and P_1 = 6 bar in red

V. CONTROLLER DESIGN

The feedforward part is based on the nominal inverse static gain of the linearized model ($G_{0\_nom} = G_0$(5 bar)) used for the design of the feedback control law, namely:

$$U_{ff}(t) = G_{0\_nom}^{-1} P_{ref}(t) \quad . \tag{31}$$

A. User specifications

The user specifications of the control system defined from a preliminary work [1] [15] are the following:

- a phase margin $M_\Phi > 40°$;
- an open-loop gain crossover frequency $\omega_u \geq 2\pi$ 10 rad/s;
- a steady-state error equal to 0;
- a variation range of U_{fb} given by $-0.45\,\text{V} \leq U_{fb} \leq 1\,\text{V}$.

B. CRONE Control-System Design (CSD) methodology

The CRONE CSD methodology is a frequency-domain approach developed since the eighties [12] [13] [15]. It is based on the common unity-feedback configuration presented in Figure 4. Three CRONE CSD methods have been developed, each one of them denotes a generation of CRONE design. The general form of the nominal open-loop transfer function β_{nom}(s) of the second generation CRONE control is defined by:

$$\beta_{nom}(s) = \beta_0 \left(\frac{1+s/\omega_l}{s/\omega_l}\right)^{n_l} \left(\frac{1+s/\omega_h}{1+s/\omega_l}\right)^{n} (1+s/\omega_h)^{-n_h} \quad .(32)$$

The first part of the above equation (32) represents the behaviour at low frequencies with an integer order n_l, the second represents the behaviour at middle frequencies with non-integer order n varying between 1 and 2 around ω_u, and the last represents the behaviour at high frequencies with an integer order n_h. As for the gain β_0, it is defined by [15]:

$$\beta_0 = (\omega_u/\omega_l)^{n_l} \left(1+(\omega_u/\omega_l)^2\right)^{(n-n_l)/2} \left(1+(\omega_u/\omega_h)^2\right)^{(n_h-n)/2} \tag{33}$$

with M_Φ = 45°, $\omega_u = 2\pi$ 10 rad/s, $G_0 \in [325\,;412.5]$ Pa/V and in accordance with the methodology described in [13], the parameter's values of the open-loop transfer function are:

$$\begin{cases} n_l = 2\,,\, n = 1.5\,,\, n_h = 2 \\ \omega_l = 5.79 \text{ rad/s}\,,\, \omega_h = 20\,444 \text{ rad/s}\,,\, \beta_0 = 32.92 \text{ SI} \end{cases} . \tag{34}$$

When the nominal open-loop transfer is determined, the fractional controller $C_F(s)$ is defined by its frequency response:

$$C_F(j\omega) = \beta_{nom}(j\omega) / G_{nom}(j\omega) \,. \tag{35}$$

The synthesis of the ideal frequency response $C_F(j\omega)$ consists of identifying a rational frequency response $C_R(j\omega)$ given by:

$$C_R(j\omega) = B(j\omega) / A(j\omega) \,, \tag{36}$$

where $B(j\omega)$ and $A(j\omega)$ are polynomials of specified integer degrees n_B and n_A. All the frequency-domain system identification techniques can be used [13].

Figure 12 presents the Bode plot of the controller $C_R(j\omega)$.

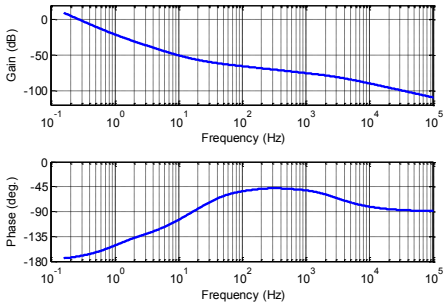

Fig. 12. Bode plot of $C_R(j\omega)$

VI. SYSTEM PERFORMANCE

A. Frequency domain

Figure 13 presents the Bode plots (a) and the Nichols loci (b) of the open-loop transfer function $\beta(j\omega)$, the Bode plots of complementary sensitivity function $T(j\omega)$ (c), of sensitivity function $S(j\omega)$ (d), of control effort sensitivity function $CS(j\omega)$ (e) and of plant input sensitivity function $GS(j\omega)$ (f) obtained with the CRONE controller for the three cases (min, nom, max). As one can observe, the phase margin M_Φ (b) and the resonant peaks Q_T of $T(j\omega)$ (c) and Q_S of $S(j\omega)$ (d) remain constant for all the cases thus showing the robustness of stability degree [13].

B. Time domain

The reference pressure $P_{ref}(t)$ is chosen such as:

$$\text{for} \begin{cases} t = 0 \text{ to } t_0,\, P_{ref}(t) = P_{ref}^e \\ t = t_0 \text{ to } t_1 = t_0 + T_0,\, P_{ref}(t) = P_{ref}^e + P_{ref}^0 \cos(2\pi\, t/T_0) \\ t = t_1 \text{ to } t_2 = 2t_0 + T_0,\, P_{ref}(t) = P_{ref}^e \end{cases} ,(37)$$

with $t_0 = 0.1$ s, $T_0 = 1$ s, $P_{ref}^e = 750$ Pa and $P_{ref}^0 = 185$ Pa.

It is important to note that the gain of the feedforward part is calculated only for the nominal case P_1 = 5 bar and that it is not adjusted when P_1 varies upstream the servo-valve.

Figure 14 presents time responses of $P_{ref}(t)$ and $P_m(t)$ (a) (b), of error signal $\varepsilon(t) = P_{ref}(t) - P_m(t)$ (c) (d), and of control signal $U_c(t)$ (e) (f) obtained without feedback (a) (c) (e) and with feedback (b) (d) (f) for the three cases (min, nom, max). We observe that the robust feedback and feedforward control system ensures a good pressure tracking (b) (d), not only for the nominal case (P_1 = 5bar), but also for the minimal (P_1 = 4 bar) and maximal (P_1 = 6 bar) cases. Without the robust

feedback control system (a) (c), pressure tracking is less effective. In all cases, the control signal $U_c(t)$ (e) (f) remains within the variation range defined by U_{min} and U_{max}.

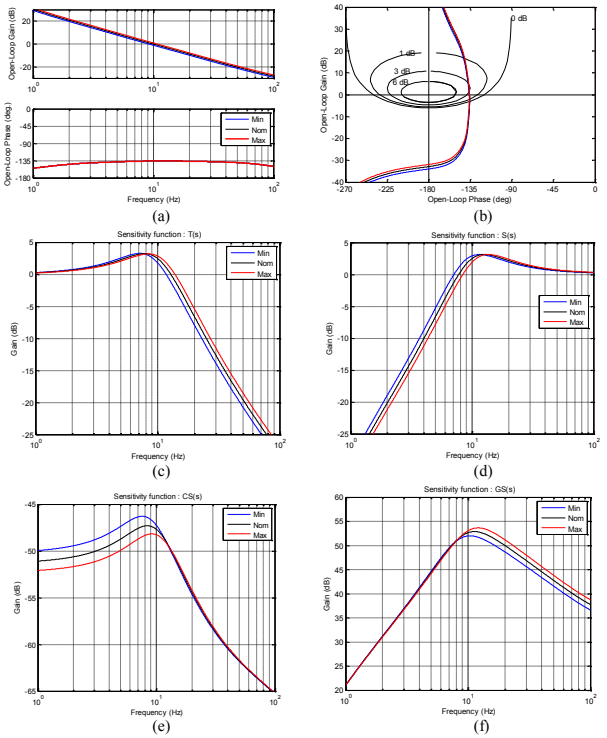

Fig. 13. Bode plots (a) and the Nichols loci (b) of $\beta(j\omega)$, Bode plots of $T(j\omega)$ (c), of $S(j\omega)$ (d), of $CS(j\omega)$ (e) and $GS(j\omega)$ (f) obtained with the CRONE controller for the three cases: min (4 bar in blue), nom (5 bar in black) and max (6 bar in red)

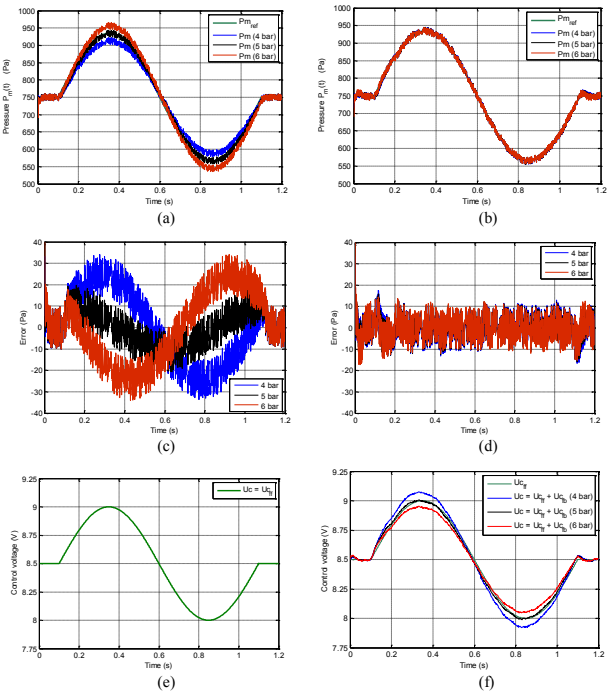

Fig. 14. Time responses of $P_{ref}(t)$ and $P_m(t)$ (a) (b), of error signal $\varepsilon(t)$ (c) (d), and of control signal $U_c(t)$ (e) (f) obtained without feedback (a) (c) (e) and with feedback (b) (d) (f) for the three cases: min (4 bar in blue), nom (5 bar in black) and max (6 bar in red)

VII. Conclusion and Future Works

The first essential step of this work is the understanding of the functioning of each component, the definition of the operating limits and the determination of the influencing physical variables. Indeed, understanding the influence of pressure P_1 on the limits of the servo-valve operating range is essential in order to be then able to define a strategy for automatic pressure P_m control inside the artificial mouth. The second important step is the design of the control architecture for a robust control of the pressure P_m. The application of the CRONE system design methodology achieves the target set with very good dynamic performance and respecting the linear operating range of the servo valve.

The objective of the future works is to include viscous thermal losses of the recorder flute in the hardware-in-the-loop simulation platform from fractional models.

VIII. Bibliography

[1] D. Ferrand and C. Vergez, "Blowing machine for wind musical instrument: toward a real-time," in *16th Mediterranean Conference on Control and Automation*, Ajaccio, France, 2008.

[2] D. Ferrand, C. Vergez , B. Fabre and F. Blanc, "High-precision regulation of a pressure controlled artificial mouth : the case of recorder-like musical instruments," *Acta Acustica united with Acustica, Hirzel Verlag,*, vol. 96, no. 4, pp. 701-712, 2010.

[3] J. Solis and A. Takanishi, "Toward understanding the nature of musical performance and interaction with wind instrument-playing humanoids," in *19th International Symposium in Robot and Human Interactive Communication*, Viareggio, 2010.

[4] M. Karjalainen and T. Maki-Patola, "Physics-based modeling of musical instruments for interactive virtual reality," in *IEEE Workshop on Multimedia Signal Processing*, Siena, Italy, 2004.

[5] R. Hamilton, "Coretet: A Dynamic Virtual Musical Instrument for the Twenty-First Century," in *IEEE Conference on Virtual Reality and 3D User Interfaces (VR)*, Osaka, Japan, 2019.

[6] G. Paine, "New Musical Instrument Design Considerations," *IEEE MultiMedia* , vol. 20, no. 4, p. IEEE MultiMedia , 2013.

[7] R. Saar, G. Levy and J. Fainguelernt, "Implementing physical models of musical instruments in the TMS320C6748," in *6th European Embedded Design in Education and Research Conference (EDERC)*, Milano, 2014.

[8] V. Chatziioannou, A. Hofmann and M. Pàmies-Vilà, "An artificial blowing machine to investigate single-reed woodwind instruments under controlled articulation conditions," in *174th Meeting of the Acoustical Society of America,* New Orleans, Louisiana, 04-08 December 2017.

[9] G. Abou Haidar, X. Moreau and R. Abi Zeid Daou, "Robust Control of an Artificial Mouth for a Wind Musical Instrument," in *International Conference on Fractional Differentiation and its Applications*, Jordan, 2018.

[10] G. Abou Haidar , R. Abi Zeid Daou and X. Moreau, "Modelling and Identification of the Musicians Blowing Part and the Flute Musical Instrument," in *Fourth International Conference on Advances in Computational Tools for Engineering Applications*, Zouk, Lebanon, 2019.

[11] D. Matignon and D. D'andréa-Novel, "Spectral and time-domain consequences of an integro-differential perturbation of the wave PDE," in *3rd WAVES conference*, Mandelieu, France, 1995.

[12] A. Oustaloup, La dérivation non entière : Théorie, synthèse et applications, Paris: Hermes, 1995.

[13] A. Oustaloup, La commande CRONE, Paris: Hermes, 1991.

[14] P. Lanusse, R. Malti and P. Melchior, "CRONE control system design toolbox for the control engineering community: tutorial and case study," *Philosophical transaction of the royal society,* vol. 391, pp. 1-14, 2013.

[15] Lanusse, P., De la commande CRONE de première génération à la commande CRONE de troisième generation, PhD Thesis, Bordeaux I University, France, 1994.

[16] Lanusse, P., CRONE Control System Design, a CRONE toolbox for Matlab, http://www.ims-bordeaux.fr/CRONE/toolbox, 2010.